Nodal-link semimetals

Zhongbo Yan,[1] Ren Bi,[1] Huitao Shen,[1,2] Ling Lu,[3] Shou-Cheng Zhang,[4] and Zhong Wang[1,*]

[1]*Institute for Advanced Study, Tsinghua University, Beijing 100084, China*
[2]*Department of Physics, Massachusetts Institute of Technology, Cambridge, Massachusetts 02139, USA*
[3]*Institute of Physics, Chinese Academy of Sciences/Beijing National Laboratory for Condensed Matter Physics, Beijing 100190, China*
[4]*Department of Physics, Stanford University, California 94305, USA*

In topological semimetals, the valance band and conduction band meet at zero-dimensional nodal points or one-dimensional nodal rings, which are protected by band topology and symmetries. In this Rapid Communication, we introduce "nodal-link semimetals", which host linked nodal rings in the Brillouin zone. We put forward a general recipe based on the Hopf map for constructing models of nodal-link semimetals. The consequences of nodal ring linking in the Landau levels and Floquet properties are investigated.

Introduction. Topological phases of matter have been among the most active research subjects in condensed matter physics. They can be broadly classified as two major classes. The first class of phases, including topological insulators and superconductors [1–6], and other symmetry protected topological phases [7], have gapped bulks with nontrivial topological structures characterized by topological invariants [8–15], dictating the existence of robust gapless modes on the boundary.

More recently, the second major class of topological materials, known as topological semimetals, have attracted widespread attention. In the noninteracting limit, they are characterized by topologically robust **k**-space band-touching manifolds, which can be zero-dimensional (0D) nodal points or one-dimensional (1D) nodal rings (or nodal lines). The bulk Dirac [16–25] and Weyl points [26–40] are responsible for novel phenomena related to chiral anomaly [41–51]. Moreover, bulk Weyl points entail surface Fermi arcs, while nodal rings [52–72] imply flat surface band (drumhead states) that may trigger interesting correlation effects [73]. Nodal rings have been predicted (e.g., Cu_3PdN [60,61], Hg_3As_2 [74], Ca_3P_2 [63,75], three-dimensional (3D) carbon networks [58], CaP_3 [76], alkaline earth metals [77,78]) and experimentally studied in quite a few materials (e.g., $PbTaSe_2$ [62], ZrSiTe [79], ZrSiS [80–84]). Notably, nodal rings can be driven to Floquet Weyl points by circularly polarized light [85–89]; accordingly, the drumhead surface states become Fermi arcs.

Unlike nodal points, nodal rings allow richer topological structures. They can touch at special points [60,61,90,91], enabling formations of nodal chains [92,93]. In this Rapid Communication, we introduce another type of topological semimetals, dubbed "nodal-link semimetals", which host nontrivially linked nodal rings [e.g., Fig. 1(e)]. Furthermore, a method is introduced for constructing two-band models of nodal-link semimetals. We investigate generic physical consequences of nontrivial linking; in particular, a global toroidal π Berry phase generates a half-integer shift of Landau level index when the magnetic field is perpendicular to the ring plane. In addition, a suitable periodic external field can drive a nodal-link semimetal to a Floquet Hopf insulator.

Models. Nodal rings come from the crossing of two adjacent bands, thus we focus on two-band Bloch Hamiltonians, which can generally be written as

$$H(\mathbf{k}) = a_0(\mathbf{k})\mathbf{1} + a_1(\mathbf{k})\tau_x + a_2(\mathbf{k})\tau_y + a_3(\mathbf{k})\tau_z, \quad (1)$$

where $\mathbf{k} = (k_x, k_y, k_z)$, τ_i's are Pauli matrices, and $a_0(\mathbf{k}) = 0$ will be adopted for simplicity (nonzero a_0 can be trivially included, if needed). Nodal rings are protected by crystal symmetries. For concreteness, we take the $\mathcal{PT}$ symmetry [66,94] that ensures the reality of $H(\mathbf{k})$, i.e., $a_2(\mathbf{k}) = 0$. Now the spectra are $E_\pm(\mathbf{k}) = \pm\sqrt{a_1^2 + a_3^2}$, and the nodal rings are given by solving $a_1(\mathbf{k}) = a_3(\mathbf{k}) = 0$. A purpose of this Rapid Communication is to construct models with mutually linked nodal rings.

Instead of taking trial-and-error approaches, we put forward a general method based on Hopf maps [95,96]. They play special roles in quantum spin systems [95,97], topological Hopf insulators [98–103], liquid-crystal solitons [104], quench dynamics of Chern insulators [105], and minimal models for topologically trivial superconductor-based Majorana zero modes [106]. Mathematically, a Hopf map is a nontrivial mapping from a three-sphere S^3 to a two-sphere S^2, which possesses a nonzero Hopf invariant [95,96,98]. Moreover, it has the geometrical property that the preimage circles of any two points on S^2 are linked. Mappings from a 3D torus T^3 to S^2 inherit the nontrivial topology of Hopf maps through $T^3 \to S^3 \to S^2$, where $T^3 \to S^3$ is a map with unit winding number, and $S^3 \to S^2$ is a Hopf map.

Given any vector function $\mathbf{d}(\mathbf{k}) = (d_x, d_y, d_z)$ on the Brillouin zone T^3, one can define a mapping from T^3 to S^2 by $\mathbf{k} \to \hat{\mathbf{d}}(\mathbf{k})$, where $\hat{\mathbf{d}} \equiv \mathbf{d}/|\mathbf{d}|$. To define the Hopf invariant, it is convenient to express the vector $\mathbf{d}$ in terms of a spinor, namely, $d_i(\mathbf{k}) = z^\dagger \tau_i z$, with $z(\mathbf{k}) = (z_1, z_2)^T$. Let us write $z_1 = N_1 + iN_2$, $z_2 = N_3 + iN_4$, then the Hopf invariant simplifies to [103]

$$n_h = \frac{1}{2\pi^2} \int d^3k \, \epsilon^{abcd} \hat{N}_a \partial_{k_x} \hat{N}_b \partial_{k_y} \hat{N}_c \partial_{k_z} \hat{N}_d, \quad (2)$$

where $\hat{N}_a$ is the ath component of the vector $\mathbf{N} = (N_1, N_2, N_3, N_4)$ normalized to unit length.

*wangzhongemail@tsinghua.edu.cn

Let us take a point on S^2, say $\hat{\mathbf{n}}_1 = (0,1,0)$. Under the mapping $\mathbf{k} \to \hat{\mathbf{d}}(\mathbf{k})$, all the preimages of $\hat{\mathbf{n}}_1$ have to satisfy

$$d_x(\mathbf{k}) = d_z(\mathbf{k}) = 0, \qquad (3)$$

however, the converse is not true, namely, a solution of Eq. (3) is not necessarily a preimage of $\hat{\mathbf{n}}_1$. In fact, the preimages of $\hat{\mathbf{n}}_2 = (0,-1,0)$ also satisfy Eq. (3). In a single equation, Eq. (3) gives the preimages of both $\hat{\mathbf{n}}_1$ and $\hat{\mathbf{n}}_2$. This is among the key observations in our construction. When n_h is nonzero, the preimage circles of any two points (say $\hat{\mathbf{n}}_1$ and $\hat{\mathbf{n}}_2$) are linked. Therefore, we can obtain linked nodal rings by taking

$$a_1(\mathbf{k}) = d_x(\mathbf{k}), \quad a_3(\mathbf{k}) = d_z(\mathbf{k}). \qquad (4)$$

Recall that the a_2 term is absent due to crystal symmetries, as discussed above. The same method also works if we start from a different $\mathbf{n}_{1,2}$; for instance, taking $\mathbf{n}_{1,2} = (0,0,\pm 1)$ leads to $a_1 = d_x$, $a_3 = d_y$, which yields a nodal link as well.

This is a quite general approach to construct nodal-link semimetals. As an example, we take [98–103]

$$N_1 = \sin k_x, \quad N_2 = \sin k_y, \quad N_3 = \sin k_z,$$
$$N_4 = \cos k_x + \cos k_y + \cos k_z - m_0, \qquad (5)$$

which has $n_h = -1$ for $1 < m_0 < 3$ and $n_h = 0$ for $m_0 > 3$. The explicit forms of d_i's read

$$d_x = 2 \sin k_x \sin k_z + 2 \sin k_y \left(\sum_{i=x,y,z} \cos k_i - m_0 \right),$$

$$d_y = -2 \sin k_y \sin k_z + 2 \sin k_x \left(\sum_{i=x,y,z} \cos k_i - m_0 \right),$$

$$d_z = \sin^2 k_x + \sin^2 k_y - \sin^2 k_z - \left(\sum_{i=x,y,z} \cos k_i - m_0 \right)^2.$$

Following Eq. (4), a lattice model of nodal-link semimetal is

$$H(\mathbf{k}) = \left[2 \sin k_x \sin k_z + 2 \sin k_y \left(\sum_{i=x,y,z} \cos k_i - m_0 \right) \right] \tau_x + \left[\sin^2 k_x + \sin^2 k_y - \sin^2 k_z - \left(\sum_{i=x,y,z} \cos k_i - m_0 \right)^2 \right] \tau_z. \qquad (6)$$

The nodal rings consist of points where both coefficients of τ_x and τ_z vanish. We find that one of the rings is $k_y = k_z$, $\sin k_x = m_0 - \sum_i \cos k_i$, and the other is $k_y = -k_z$, $\sin k_x = \sum_i \cos k_i - m_0$, shown in light and dark blue, respectively, in Fig. 1. Figure 1(a) shows the unlinked rings for $m_0 = 3.2$, and Fig. 1(e) illustrates the linked rings for $m_0 = 2.5$ (a Hopf link). The critical point $m_0 = 3.0$, when the two rings cross each other, is shown in Fig. 1(c). The direction of pseudospin vector (d_x, d_z) is plotted in Figs. 1(b), 1(d) and 1(f), indicating that the light-blue ring encloses a pseudospin vortex in the linked regime [Fig. 1(f)], in contrast to the unlinked case [Fig. 1(b)]. The surface states for $m_0 = 2.5$ are shown in Fig. 2. The two-disk-overlapping region has zero and two flat bands in Figs. 2(a) and 2(c), respectively, which is consistent with the winding number [107] in each region.

Near the critical point [Fig. 1(c)], we can expand the Hamiltonian as

$$H(\mathbf{k}) = [2k_x k_z + 2k_y(m - k^2/2)]\tau_x$$
$$+ [k_x^2 + k_y^2 - k_z^2 - (m - k^2/2)^2]\tau_z, \qquad (7)$$

where $k^2 = \sum_{i=x,y,z} k_i^2$, $m = 3 - m_0$. At the critical point $m = 0$, we have $H(\mathbf{k}) \approx 2k_x k_z \tau_x + (k_x^2 + k_y^2 - k_z^2)\tau_z$, thus the dispersion is quadratic in all three directions. Consequently, we find that, for $m = 0$, the density of states follows $g(E) \sim \sqrt{E}$ near zero energy, in contrast to $g(E) \sim E$ for $m \neq 0$. Just like the nontrivial topology of insulators can be undone by closing the energy gap, the nontrivial nodal-line linking can be untied through quadratic-dispersion critical points [Fig. 1(c)], where $g(E) \sim \sqrt{E}$.

We remark that, although a nodal chain [92,93] also contains crossings like Fig. 1(c), its dispersion is not quadratic in all three directions at the crossing point, and the density of states is linear instead of square root.

Landau levels. A key difference between a usual unlinked ring and a linked one is a global Berry phase along the ring. Let us draw a thin torus enclosing a nodal ring, then the Berry phase along the poloidal direction is always π; in contrast, the Berry phase along the toroidal direction can be 0 or π (mod 2π), corresponding to the unlinked and linked ring, respectively. [The 0 or π toroidal Berry phase of the light-blue ring can be read from the spin texture in Figs. 1(b) and 1(f), respectively.]

This π toroidal Berry phase can qualitatively affect the Landau levels. It is challenging to find analytic expressions of Landau levels for Eq. (6), nevertheless, a different model allows a simple solution: we take $a_1 = d_x(\mathbf{k})$, $a_3 = d_y(\mathbf{k})$ in Eq. (1). This Bloch Hamiltonian harbors four straight nodal lines at $(k_x, k_y) = (0,0)$, $(0,\pi)$, $(0,\pi)$, and (π,π), respectively. When $1 < m_0 < 3$, a nodal ring encircling $(k_x, k_y) = (0,0)$ is also found as $\cos k_x + \cos k_y = m_0 - 1$ in the $k_z = 0$ plane. Instead of working on this lattice Hamiltonian, we study its continuum limit for simplicity:

$$H(\mathbf{k}) = 2[k_x k_z + (m - Ck^2)k_y]\tau_x$$
$$+ 2[-k_y k_z + (m - Ck^2)k_x]\tau_y, \qquad (8)$$

where $k^2 = k_x^2 + k_y^2 + k_z^2$, $m = 3 - m_0$, and $C = 0.5$. We have also done a basis change $\tau_z \to \tau_y$ for later convenience. This model hosts a nodal line $k_x = k_y = 0$ and a nodal ring $k_x^2 + k_y^2 = m/C$ in the $k_z = 0$ plane, which are linked.
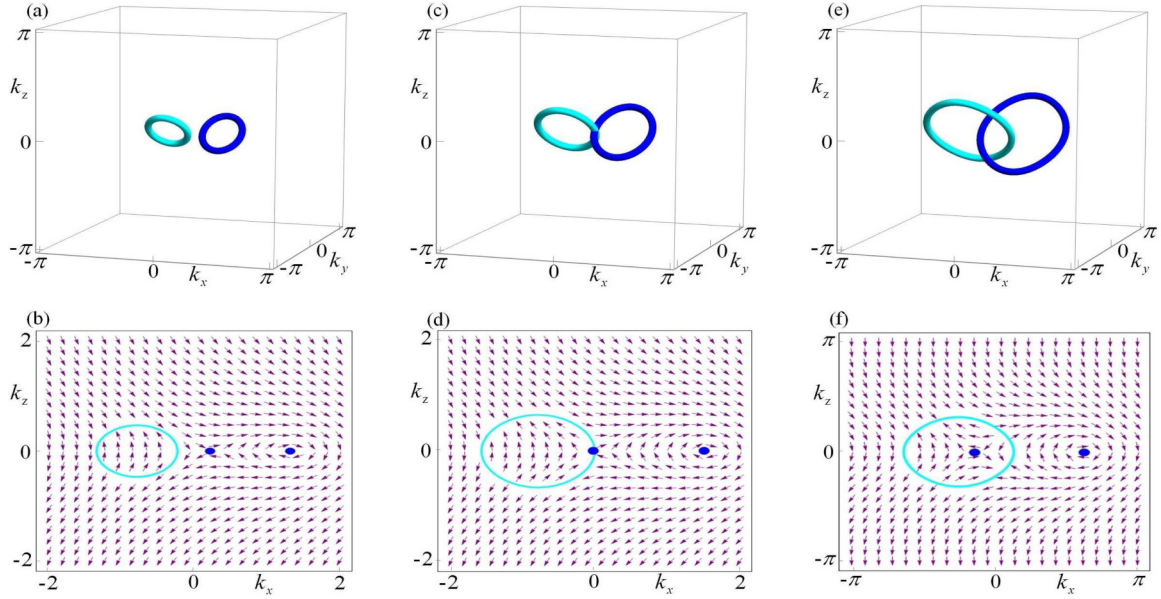
FIG. 1. Nodal rings of Eq. (6), and the pseudospin textures in the $k_y = k_z$ plane, for [(a),(b)] $m_0 = 3.2$, [(c),(d)] $m_0 = 3.0$, and [(e),(f)] $m_0 = 2.5$. The light-blue ring locates in the $k_y = k_z$ plane, while the dark-blue ring is perpendicular to it.

Now we add a magnetic field along the z direction, $\mathbf{B} = B\hat{z}$. It is standard to do the replacement $\mathbf{k} \to \Pi = -i\nabla + e\mathbf{A}$ with $\mathbf{A} = (0, Bx, 0)$ [108]. It is convenient to introduce the ladder operators, $a = \frac{l_B}{\sqrt{2}}(\Pi_x - i\Pi_y)$, $a^\dagger = \frac{l_B}{\sqrt{2}}(\Pi_x + i\Pi_y)$, where $l_B = 1/\sqrt{eB}$ is the magnetic length. The Hamiltonian becomes

$$H = \begin{pmatrix} 0 & f(k_z)\frac{\sqrt{2}a^\dagger}{l_B} \\ \frac{\sqrt{2}a}{l_B}f^\dagger(k_z) & 0 \end{pmatrix} \quad (9)$$

where $f(k_z) = 2[k_z - i(m - Ck_z^2 - \frac{2Ca^\dagger a}{l_B^2})]$. The Landau levels are found to be

$$E_{n,\pm}(k_z) = \begin{cases} \pm\sqrt{8n[k_z^2 + (m - Ck_z^2 - n\omega_c)^2]}/l_B, & n \geqslant 1, \\ 0, & n = 0, \end{cases}$$
(10)

where $\omega_c \equiv 2C/l_B^2$. The low-energy eigenvalues are around $n \sim 0$ and $n \sim m/\omega_c$, the former coming from the central
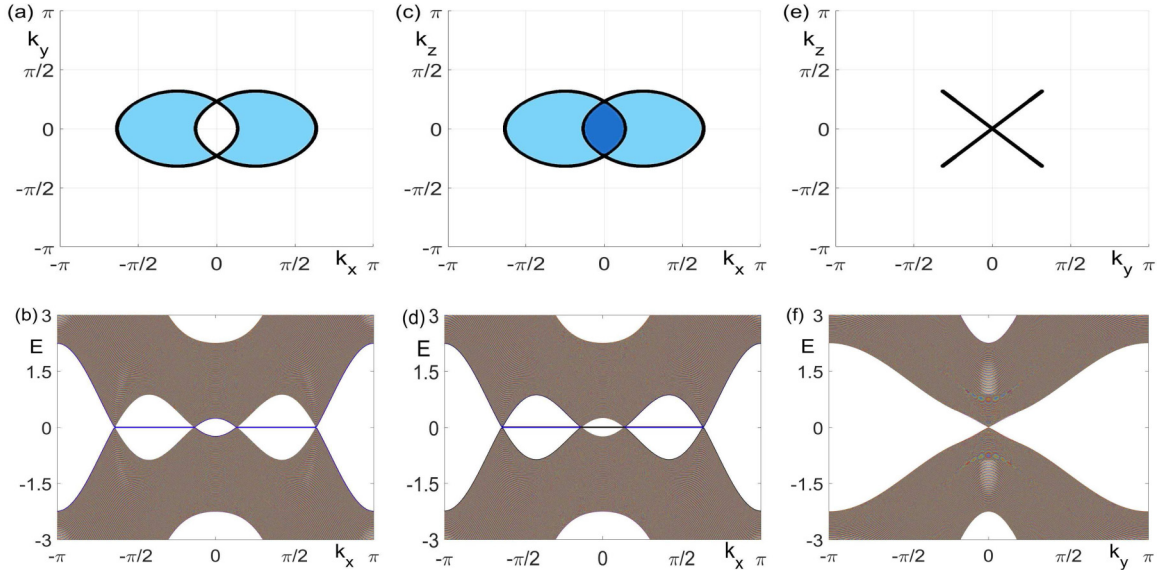

FIG. 2. (a) Surface flat bands for $z = 0$ boundary. (b) The spectra as a function of k_x (fixed $k_y = 0$) for an 800-site-thick slab perpendicular to the z axis. (c) The $y = 0$ surface states. (d) Spectra of a slab perpendicular to the y axis. (e) $x = 0$ surface Brillouin zone without surface states. (f) Spectra of a slab perpendicular to the x axis. The black rings or lines in (a), (c), and (e) are projections of the bulk nodal link to the surface Brillouin zone. In (c), the number of bands in the two-disk-overlapping region is twice that of the nonoverlapping regions. Here, $m_0 = 2.5$.

nodal line at $k_x = k_y = 0$, while the latter coming from the nodal ring in the $k_z = 0$ plane. As a comparison, we also consider a model with an unlinked ring:

$$H(\mathbf{k}) = (m - Ck^2)\tau_x + k_z\tau_z. \qquad (11)$$

Following the same steps, we find that the Landau levels are

$$E_{n,\pm}(k_z) = \pm\sqrt{k_z^2 + \left[m - Ck_z^2 - \left(n + \tfrac{1}{2}\right)\omega_c\right]^2}, \quad n \geq 0. \quad (12)$$

Comparing Eq. (10) and Eq. (12), we see that the presence of a linked nodal line causes a shift of Landau level index by $1/2$, namely, $n \to n - 1/2$, which is a consequence of the π toroidal Berry phase. Such a shift can be measured by magnetotransport or magneto-optical experiments.

To highlight the effect of π Berry phase, we rederive the Landau levels using semiclassical quantization [109–111]:

$$S(k_z) = 2\pi eB(n + 1/2 - \phi_B/2\pi), \qquad (13)$$

where S is the cross-sectional area of a $\mathbf{k}$-space orbit, and ϕ_B is the Berry phase along the orbit. For the linked ring, we have $\phi_B = \pi$ (the toroidal Berry phase), and a semiclassical calculation (see Supplemental Material for details [112]) yields the Landau levels in Eq. (10).

Floquet Hopf insulator from nodal link. We will show that driving the nodal-link semimetal described by Eq. (8) creates a Floquet Hopf insulator. We consider a periodic driving generated by a circularly polarized light (CPL) propagating in the z direction. The vector potential $\mathbf{A}(t) = A_0(\cos\omega t, \eta\sin\omega t, 0)$, where $\eta = 1$ and -1 stands for right-handed and left-handed CPL, respectively. Its effect is described by the minimal coupling, $H(\mathbf{k}) \to H[\mathbf{k} + e\mathbf{A}(t)]$. The full Hamiltonian is time-periodic, $H(\mathbf{k}, t + T) = H(\mathbf{k}, t)$ with $T = 2\pi/\omega$, thus it can be expanded as $H(\mathbf{k}, t) = \sum_n \mathcal{H}_n(\mathbf{k})e^{in\omega t}$, with

$$\mathcal{H}_0(\mathbf{k}) = 2[k_x k_z + k_y(\tilde{m}_2 - Ck^2)]\tau_x$$
$$+ 2[-k_y k_z + k_x(\tilde{m}_2 - Ck^2)]\tau_y,$$

$$\mathcal{H}_{\pm 1}(\mathbf{k}) = eA_0[k_z \mp i\eta(\tilde{m}_1 - Ck^2) - 2Ck_y(k_x \mp i\eta k_y)]\tau_x$$
$$+ eA_0[\pm i\eta k_z + (\tilde{m}_1 - Ck^2) - 2Ck_x(k_x \mp i\eta k_y)]\tau_y,$$

$$\mathcal{H}_{\pm 2}(\mathbf{k}) = Ce^2 A_0^2[(k_y \pm i\eta k_x)\tau_x - (k_x \mp i\eta k_y)\tau_y], \qquad (14)$$

where $\tilde{m}_{j=1,2} = m - jCe^2 A_0^2$. In the off-resonance regime, we can use an effective time-independent Hamiltonian [113–121]:

$$H_{\text{eff}}(\mathbf{k}) = \mathcal{H}_0 + \sum_{n\geq 1}\frac{[\mathcal{H}_n, \mathcal{H}_{-n}]}{n\omega} + O\left(\frac{1}{\omega^2}\right)$$

$$= 2[k_x k_z + k_y(\tilde{m}_2 - Ck^2)]\tau_x$$
$$+ 2[-k_y k_z + k_x(\tilde{m}_2 - Ck^2)]\tau_y$$
$$+ \lambda\bigg[k_z^2 + (\tilde{m}_1 - Ck^2)^2$$
$$- 2Ck_\rho^2\left(\tilde{m}_1 - Ck^2 - \frac{\gamma}{4}\right)\bigg]\tau_z, \qquad (15)$$

where $\lambda = 4\eta e^2 A_0^2/\omega$, $\gamma = Ce^2 A_0^2$, and $k_\rho = \sqrt{k_x^2 + k_y^2}$. The energy spectrum of H_{eff} is fully gapped. For weak driving, the minima of the band are located at $k_z = 0$, $Ck_\rho^2 = \tilde{m}_2$, and the gap is estimated as $E_g \approx 12mC(eA_0)^4/\omega$. In the CPL approach, this gap is expected to be rather small. It can
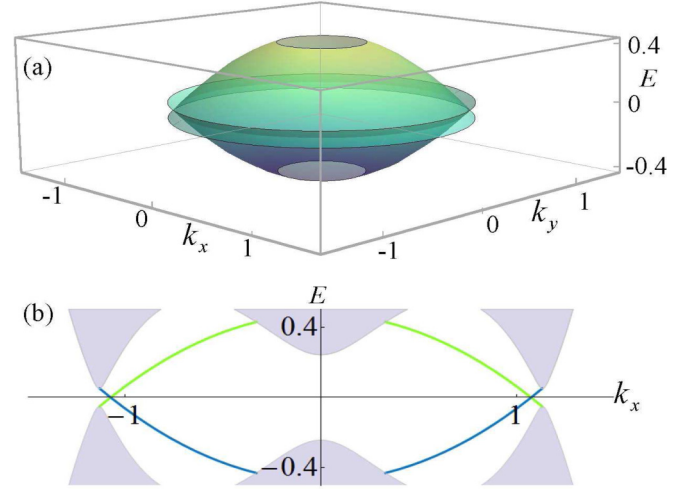

FIG. 3. Surface states of a slab perpendicular to the z axis. Parameters are $\omega = 4$, $m = 1$, $eA_0 = 0.6$, $C = 0.5$. (a) 3D view of surface bands. (b) $E(k_x)$ with $k_y = 0$ fixed. The gray regions are bulk bands.

be promoted to the order of $(eA_0)^2$ by adding a small $\Delta\tau_z$ pseudo-Zeeman term (see Supplemental Material for details of calculation).

If we remove the τ_z term, Eq. (15) hosts a nodal ring and a nodal line linked together. It is readily checked that the coefficient of τ_z is positive on the line and negative on the ring (for $\eta = +1$), thus the corresponding unit $\hat{\mathbf{d}}$ vector is $(0,0,1)$ and $(0,0,-1)$, respectively. This fact suggests that Eq. (15) describes a (Floquet) Hopf insulator [98–103], or more precisely, a Floquet Hopf-Chern insulator [102], because the Chern number $C(k_z) = -2$ for arbitrary k_z, as found in our numerical calculation. In the definition of Hopf invariant [95,98], a nonsingular global Berry potential is needed, which is impossible in the presence of a nonzero Chern number, nevertheless, we can study topological surface states. For a slab perpendicular to the z direction, we can solve the differential equation $H_{\text{eff}}(k_x, k_y, -i\partial_z)\Psi_{k_x,k_y}(z) = E(k_x, k_y)\Psi_{k_x,k_y}(z)$, which gives one surface band for each surface, whose dispersion is (see Supplemental Material for calculation) $E_\alpha(\mathbf{k}) = \alpha\lambda[\tilde{m}_2/C + \gamma^2 - (1 + 3C\gamma/2)k_\rho^2]$, where $\alpha = +(-)$ for the top (bottom) surface. Shown in Fig. 3, this dispersion is characteristic of a Hopf insulator [98]. For a fixed θ (defined as $\theta = \arctan k_y/k_x$), the surface state of either the top or bottom surface is chiral, which can be understood in terms of a Chern number in the (k_ρ, k_z) space [103].

Conclusions. We have introduced nodal-link semimetals into the family of topological semimetals. A general method for their model construction has been put forward. These phases may be realized by tuning the hoppings in optical lattices. Finding a solid-state material will be important progress. It will also be worthwhile to study possible novel effects of linking. Theoretically, our models lay useful groundwork for topological field theories [122] in the Brillouin zone.

Note added. Recently, we became aware of a related eprint by Chen *et al.*, in which a double-helix link is constructed without using the Hopf map [123]. In another recent work, the Hopf map method has been generalized by Ezawa to construct other nodal links [124].

[1] M. Z. Hasan and C. L. Kane, *Colloquium*: Topological insulators, Rev. Mod. Phys. **82**, 3045 (2010).

[2] X.-L. Qi and S.-C. Zhang, Topological insulators and superconductors, Rev. Mod. Phys. **83**, 1057 (2011).

[3] C.-K. Chiu, J. C. Y. Teo, A. P. Schnyder, and S. Ryu, Classification of topological quantum matter with symmetries, Rev. Mod. Phys. **88**, 035005 (2016).

[4] A. Bansil, H. Lin, and T. Das, *Colloquium*: Topological band theory, Rev. Mod. Phys. **88**, 021004 (2016).

[5] B. A. Bernevig and T. L. Hughes, *Topological Insulators and Topological Superconductors* (Princeton University Press, Princeton, NJ, 2013).

[6] S.-Q. Shen, *Topological Insulators: Dirac Equation In Condensed Matters*, Vol. 174 (Springer Science & Business Media, Berlin, 2013).

[7] X. Chen, Z.-C. Gu, Z.-X. Liu, and X.-G. Wen, Symmetry protected topological orders and the group cohomology of their symmetry group, Phys. Rev. B **87**, 155114 (2013).

[8] D. J. Thouless, M. Kohmoto, M. P. Nightingale, and M. den Nijs, Quantized Hall Conductance in a Two-Dimensional Periodic Potential, Phys. Rev. Lett. **49**, 405 (1982).

[9] Q. Niu, D. J. Thouless, and Y.-S. Wu, Quantized Hall conductance as a topological invariant, Phys. Rev. B **31**, 3372 (1985).

[10] C. L. Kane and E. J. Mele, Z_2 Topological Order and the Quantum Spin Hall Effect, Phys. Rev. Lett. **95**, 146802 (2005).

[11] L. Fu, C. L. Kane, and E. J. Mele, Topological Insulators in Three Dimensions, Phys. Rev. Lett. **98**, 106803 (2007).

[12] J. E. Moore and L. Balents, Topological invariants of time-reversal-invariant band structures, Phys. Rev. B **75**, 121306 (2007).

[13] X.-L. Qi, T. Hughes, and S.-C. Zhang, Topological field theory of time-reversal invariant insulators, Phys. Rev. B **78**, 195424 (2008).

[14] A. P. Schnyder, S. Ryu, A. Furusaki, and A. W. W. Ludwig, Classification of topological insulators and superconductors in three spatial dimensions, Phys. Rev. B **78**, 195125 (2008).

[15] Z. Wang and S.-C. Zhang, Simplified Topological Invariants for Interacting Insulators, Phys. Rev. X **2**, 031008 (2012).

[16] Z. K. Liu, B. Zhou, Y. Zhang, Z. J. Wang, H. M. Weng, D. Prabhakaran, S.-K. Mo, Z. X. Shen, Z. Fang, X. Dai *et al.*, Discovery of a three-dimensional topological Dirac semimetal, Na$_3$Bi, Science **343**, 864 (2014).

[17] M. Neupane, S.-Y. Xu, R. Sankar, N. Alidoust, G. Bian, C. Liu, I. Belopolski, T.-R. Chang, H.-T. Jeng, H. Lin, A. Bansil, F. Chou, and M. Z. Hasan, Observation of a three-dimensional topological Dirac semimetal phase in high-mobility Cd$_3$As$_2$, Nat. Commun. **5**, 3786 (2014).

[18] S. Borisenko, Q. Gibson, D. Evtushinsky, V. Zabolotnyy, B. Büchner, and R. J. Cava, Experimental Realization of a Three-Dimensional Dirac Semimetal, Phys. Rev. Lett. **113**, 027603 (2014).

[19] S.-Y. Xu, C. Liu, S. K. Kushwaha, R. Sankar, J. W. Krizan, I. Belopolski, M. Neupane, G. Bian, N. Alidoust, T.-R. Chang *et al.*, Observation of Fermi arc surface states in a topological metal, Science **347**, 294 (2015).

[20] S. M. Young, S. Zaheer, J. C. Y. Teo, C. L. Kane, E. J. Mele, and A. M. Rappe, Dirac Semimetal in Three Dimensions, Phys. Rev. Lett. **108**, 140405 (2012).

[21] Z. Wang, Y. Sun, X.-Q. Chen, C. Franchini, G. Xu, H. Weng, X. Dai, and Z. Fang, Dirac semimetal and topological phase transitions in A_3Bi (A = Na, K, Rb), Phys. Rev. B **85**, 195320 (2012).

[22] Z. Wang, H. Weng, Q. Wu, X. Dai, and Z. Fang, Three-dimensional Dirac semimetal and quantum transport in Cd$_3$As$_2$, Phys. Rev. B **88**, 125427 (2013).

[23] C. Zhang, E. Zhang, Y. Liu, Z.-G. Chen, S. Liang, J. Cao, X. Yuan, L. Tang, Q. Li, T. Gu, Y. Wu, J. Zou, and F. Xiu, Detection of chiral anomaly and valley transport in Dirac semimetals, arXiv:1504.07698.

[24] R. Y. Chen, Z. G. Chen, X.-Y. Song, J. A. Schneeloch, G. D. Gu, F. Wang, and N. L. Wang, Magnetoinfrared Spectroscopy of Landau Levels and Zeeman Splitting of Three-Dimensional Massless Dirac Fermions in ZrTe$_5$, Phys. Rev. Lett. **115**, 176404 (2015).

[25] Y. Liu, X. Yuan, C. Zhang, Z. Jin, A. Narayan, C. Luo, Z. Chen, L. Yang, J. Zou, X. Wu *et al.*, Zeeman splitting and dynamical mass generation in Dirac semimetal ZrTe$_5$, Nat. Commun. **7**, 12516 (2016).

[26] X. Wan, A. M. Turner, A. Vishwanath, and S. Y. Savrasov, Topological semimetal and Fermi-arc surface states in the electronic structure of pyrochlore iridates, Phys. Rev. B **83**, 205101 (2011).

[27] G. E. Volovik, *The Universe in a Helium Droplet* (Oxford University Press, New York, 2003).

[28] K.-Y. Yang, Y.-M. Lu, and Y. Ran, Quantum Hall effects in a Weyl semimetal: Possible application in pyrochlore iridates, Phys. Rev. B **84**, 075129 (2011).

[29] A. A. Burkov and L. Balents, Weyl Semimetal in a Topological Insulator Multilayer, Phys. Rev. Lett. **107**, 127205 (2011).

[30] H. Weng, C. Fang, Z. Fang, B. A. Bernevig, and X. Dai, Weyl Semimetal Phase in Noncentrosymmetric Transition-Metal Monophosphides, Phys. Rev. X **5**, 011029 (2015).

[31] S.-M. Huang, S.-Y. Xu, I. Belopolski, C.-C. Lee, G. Chang, B. Wang, N. Alidoust, G. Bian, M. Neupane, C.-L. Zhang, S. Jia, A. Bansil, H. Lin, and M. Z. Hasan, A Weyl Fermion semimetal with surface Fermi arcs in the transition metal monopnictide TaAs class, Nat. Commun. **6**, 7373 (2015).

[32] S.-Y. Xu, I. Belopolski, N. Alidoust, M. Neupane, G. Bian, C. Zhang, R. Sankar, G. Chang, Z. Yuan, C.-C. Lee *et al.*, Discovery of a Weyl fermion semimetal and topological Fermi arcs, Science **349**, 613 (2015).

[33] B. Q. Lv, H. M. Weng, B. B. Fu, X. P. Wang, H. Miao, J. Ma, P. Richard, X. C. Huang, L. X. Zhao, G. F. Chen *et al.*, Experimental Discovery of Weyl Semimetal TaAs, Phys. Rev. X **5**, 031013 (2015).

[34] L. X. Yang, Z. K. Liu, Y. Sun, H. Peng, H. F. Yang, T. Zhang, B. Zhou, Y. Zhang, Y. F. Guo, M. Rahn *et al.*, Weyl semimetal phase in the non-centrosymmetric compound TaAs, Nat. Phys. **11**, 728 (2015).

[35] X. Huang, L. Zhao, Y. Long, P. Wang, D. Chen, Z. Yang, H. Liang, M. Xue, H. Weng, Z. Fang, X. Dai, and G. Chen, Observation of the Chiral-Anomaly-Induced Negative Magnetoresistance in 3D Weyl Semimetal TaAs, Phys. Rev. X **5**, 031023 (2015).

[36] S.-Y. Xu, N. Alidoust, I. Belopolski, C. Zhang, G. Bian, T.-R. Chang, H. Zheng, V. Strokov, D. S. Sanchez, G. Chang, Z. Yuan, D. Mou, Y. Wu, L. Huang, C.-C. Lee, S.-M. Huang, B. Wang, A. Bansil, H.-T. Jeng, T. Neupert, A. Kaminski, H. Lin, S. Jia, and M. Z. Hasan, Discovery of Weyl semimetal NbAs, Nat. Phys. **11**, 748 (2015).

[37] C. Shekhar, A. K. Nayak, Y. Sun, M. Schmidt, M. Nicklas, I. Leermakers, U. Zeitler, Y. Skourski, J. Wosnitza, Z. Liu *et al.*, Extremely large magnetoresistance and ultrahigh mobility in the topological Weyl semimetal candidate NbP, Nat. Phys. **11**, 645 (2015).

[38] L. Lu, L. Fu, J. D. Joannopoulos, and M. Soljačić, Weyl points and line nodes in gyroid photonic crystals, Nat. Photon. **7**, 294 (2013).

[39] L. Lu, Z. Wang, D. Ye, L. Ran, L. Fu, J. D. Joannopoulos, and M. Soljačić, Experimental observation of Weyl points, Science **349**, 622 (2015).

[40] A. A. Soluyanov, D. Gresch, Z. Wang, Q. Wu, M. Troyer, X. Dai, and B. A. Bernevig, Type-II Weyl semimetals, Nature (London) **527**, 495 (2015).

[41] D. T. Son and B. Z. Spivak, Chiral anomaly and classical negative magnetoresistance of Weyl metals, Phys. Rev. B **88**, 104412 (2013).

[42] C.-X. Liu, P. Ye, and X.-L. Qi, Chiral gauge field and axial anomaly in a Weyl semimetal, Phys. Rev. B **87**, 235306 (2013).

[43] V. Aji, Adler-Bell-Jackiw anomaly in Weyl semimetals: Application to pyrochlore iridates, Phys. Rev. B **85**, 241101 (2012).

[44] A. A. Zyuzin and A. A. Burkov, Topological response in Weyl semimetals and the chiral anomaly, Phys. Rev. B **86**, 115133 (2012).

[45] Z. Wang and S.-C. Zhang, Chiral anomaly, charge density waves, and axion strings from Weyl semimetals, Phys. Rev. B **87**, 161107 (2013).

[46] P. Hosur and X. Qi, Recent developments in transport phenomena in Weyl semimetals, C. R. Phys. **14**, 857 (2013).

[47] P. Hosur and X.-L. Qi, Tunable circular dichroism due to the chiral anomaly in Weyl semimetals, Phys. Rev. B **91**, 081106 (2015).

[48] H.-J. Kim, K.-S. Kim, J.-F. Wang, M. Sasaki, N. Satoh, A. Ohnishi, M. Kitaura, M. Yang, and L. Li, Dirac versus Weyl Fermions in Topological Insulators: Adler-Bell-Jackiw Anomaly in Transport Phenomena, Phys. Rev. Lett. **111**, 246603 (2013).

[49] S. A. Parameswaran, T. Grover, D. A. Abanin, D. A. Pesin, and A. Vishwanath, Probing the Chiral Anomaly with Nonlo-cal Transport in Three-Dimensional Topological Semimetals, Phys. Rev. X **4**, 031035 (2014).

[50] Q. Li, D. E. Kharzeev, C. Zhang, Y. Huang, I. Pletikosić, A. V. Fedorov, R. D. Zhong, J. A. Schneeloch, G. D. Gu, and T. Valla, Chiral magnetic effect in ZrTe$_5$, Nat. Phys. **12**, 550 (2016).

[51] R. Bi and Z. Wang, Unidirectional transport in electronic and photonic Weyl materials by Dirac mass engineering, Phys. Rev. B **92**, 241109 (2015).

[52] A. A. Burkov, M. D. Hook, and L. Balents, Topological nodal semimetals, Phys. Rev. B **84**, 235126 (2011).

[53] J.-M. Carter, V. V. Shankar, M. A. Zeb, and H.-Y. Kee, Semimetal and topological insulator in perovskite iridates, Phys. Rev. B **85**, 115105 (2012).

[54] M. Phillips and V. Aji, Tunable line node semimetals, Phys. Rev. B **90**, 115111 (2014).

[55] M. Zeng, C. Fang, G. Chang, Y.-A. Chen, T. Hsieh, A. Bansil, H. Lin, and L. Fu, Topological semimetals and topological insulators in rare earth monopnictides, arXiv:1504.03492.

[56] Y. Chen, Y.-M. Lu, and H.-Y. Kee, Topological crystalline metal in orthorhombic perovskite iridates, Nat. Commun. **6**, 6593 (2015).

[57] C.-K. Chiu and A. P. Schnyder, Classification of reflection-symmetry-protected topological semimetals and nodal super-conductors, Phys. Rev. B **90**, 205136 (2014).

[58] H. Weng, Y. Liang, Q. Xu, R. Yu, Z. Fang, X. Dai, and Y. Kawazoe, Topological node-line semimetal in three-dimensional graphene networks, Phys. Rev. B **92**, 045108 (2015).

[59] K. Mullen, B. Uchoa, and D. T. Glatzhofer, Line of Dirac Nodes in Hyperhoneycomb Lattices, Phys. Rev. Lett. **115**, 026403 (2015).

[60] R. Yu, H. Weng, Z. Fang, X. Dai, and X. Hu, Topological Node-Line Semimetal and Dirac Semimetal State in Antiperovskite Cu$_3$PdN, Phys. Rev. Lett. **115**, 036807 (2015).

[61] Y. Kim, B. J. Wieder, C. L. Kane, and A. M. Rappe, Dirac Line Nodes in Inversion-Symmetric Crystals, Phys. Rev. Lett. **115**, 036806 (2015).

[62] G. Bian, T.-R. Chang, R. Sankar, S.-Y. Xu, H. Zheng, T. Neupert, C.-K. Chiu, S.-M. Huang, G. Chang, I. Belopolski, D. S. Sanchez, M. Neupane, N. Alidoust, C. Liu, B. Wang, C.-C. Lee, H.-T. Jeng, A. Bansil, F. Chou, H. Lin, and M. Z. Hasan, Topological nodal-line fermions in spin-orbit metal PbTaSe$_2$, Nat. Commun. **7**, 10556 (2016).

[63] L. S. Xie, L. M. Schoop, E. M. Seibel, Q. D. Gibson, W. Xie, and R. J. Cava, A new form of Ca$_3$P$_2$ with a ring of Dirac nodes, APL Mater. **3**, 083602 (2015).

[64] J.-W. Rhim and Y. B. Kim, Landau level quantization and almost flat modes in three-dimensional semimetals with nodal ring spectra, Phys. Rev. B **92**, 045126 (2015).

[65] Y. Chen, Y. Xie, S. A. Yang, H. Pan, F. Zhang, M. L. Cohen, and S. Zhang, Spin-orbit-free Weyl-loop and Weyl-point semimetals in a stable three-dimensional carbon allotrope, Nano Lett. **15**, 6974 (2015).

[66] C. Fang, Y. Chen, H.-Y. Kee, and L. Fu, Topological nodal line semimetals with and without spin-orbital coupling, Phys. Rev. B **92**, 081201 (2015).

[67] G. Bian, T.-R. Chang, H. Zheng, S. Velury, S.-Y. Xu, T. Neupert, C.-K. Chiu, S.-M. Huang, D. S. Sanchez, I. Belopolski, N. Alidoust, P.-J. Chen, G. Chang, A. Bansil, H.-T. Jeng, H. Lin, and M. Z. Hasan, Drumhead surface states and

topological nodal-line fermions in TlTaSe$_2$, Phys. Rev. B **93**, 121113(R) (2016).

[68] R. Yu, Z. Fang, X. Dai, and H. Weng, Topological nodal line semimetals predicted from first-principles calculations, Front. Phys. **12**, 127202 (2017).

[69] J.-W. Rhim and Y. B. Kim, Anisotropic density fluctuations, plasmons, and Friedel oscillations in nodal line semimetal, New J. Phys. **18**, 043010 (2016).

[70] Z. Yan, P.-W. Huang, and Z. Wang, Collective modes in nodal line semimetals, Phys. Rev. B **93**, 085138 (2016).

[71] L.-K. Lim and R. Moessner, Pseudospin Vortex Ring with a Nodal Line in Three Dimensions, Phys. Rev. Lett. **118**, 016401 (2017).

[72] C. Fang, H. Weng, X. Dai, and Z. Fang, Topological nodal line semimetals, Chin. Phys. B **25**, 117106 (2016).

[73] J. Liu and L. Balents, Correlation effects and quantum oscillations in topological nodal-loop semimetals, Phys. Rev. B **95**, 075426 (2017).

[74] J. L. Lu, W. Luo, X. Y. Li, S. Q. Yang, J. X. Cao, X. G. Gong, and H. J. Xiang, Two-dimensional node-line semimetals in a honeycomb-kagome lattice, Chin. Phys. Lett. **34**, 057302 (2017).

[75] Y.-H. Chan, C.-K. Chiu, M. Y. Chou, and A. P. Schnyder, Ca$_3$P$_2$ and other topological semimetals with line nodes and drumhead surface states, Phys. Rev. B **93**, 205132 (2016).

[76] Q. Xu, R. Yu, Z. Fang, X. Dai, and H. Weng, Topological nodal line semimetals in the CaP$_3$ family of materials, Phys. Rev. B **95**, 045136 (2017).

[77] R. Li, H. Ma, X. Cheng, S. Wang, D. Li, Z. Zhang, Y. Li, and X.-Q. Chen, Dirac Node Lines in Pure Alkali Earth Metals, Phys. Rev. Lett. **117**, 096401 (2016).

[78] M. Hirayama, R. Okugawa, T. Miyake, and S. Murakami, Topological Dirac nodal lines and surface charges in fcc alkaline earth metals, Nat. Commun. **8**, 14022 (2017).

[79] J. Hu, Z. Tang, J. Liu, X. Liu, Y. Zhu, D. Graf, Y. Shi, S. Che, C. N. Lau, J. Wei *et al.*, Topological Nodal-Line Fermions in ZrSiSe and ZrSiTe, Phys. Rev. Lett. **117**, 016602 (2016).

[80] L. M. Schoop, M. N. Ali, C. Straßer, V. Duppel, S. S. P. Parkin, B. V. Lotsch, and C. R. Ast, Dirac cone protected by non-symmorphic symmetry and 3D Dirac line node in ZrSiS, Nat. Commun. **7**, 11696 (2016).

[81] R. Singha, A. Pariari, B. Satpati, and P. Mandal, Titanic magnetoresistance and signature of non-degenerate Dirac nodes in ZrSiS, Proc. Natl. Acad. Sci. USA **114**, 2468 (2017).

[82] M. Neupane, I. Belopolski, M. M. Hosen, D. S. Sanchez, R. Sankar, M. Szlawska, S.-Y. Xu, K. Dimitri, N. Dhakal, P. Maldonado, P. M. Oppeneer, D. Kaczorowski, F. Chou, M. Z. Hasan, and T. Durakiewicz, Observation of topological nodal fermion semimetal phase in ZrSiS, Phys. Rev. B **93**, 201104(R) (2016).

[83] X. Wang, X. Pan, M. Gao, J. Yu, J. Jiang, J. Zhang, H. Zuo, M. Zhang, Z. Wei, W. Niu, Z. Xia, X. Wan, Y. Chen, F. Song, Y. Xu, B. Wang, G. Wang, and R. Zhang, Evidence of both surface and bulk Dirac bands in ZrSiS and the unconventional magnetoresistance, Adv. Electron. Mater. **2**, 1600228 (2016).

[84] C. Chen, X. Xu, J. Jiang, S.-C. Wu, Y. P. Qi, L. X. Yang, M. X. Wang, Y. Sun, N. B. M. Schröter, H. F. Yang *et al.*, Dirac line nodes and effect of spin-orbit coupling in

the nonsymmorphic critical semimetals mSiS (m = Hf, Zr), Phys. Rev. B **95**, 125126 (2017).

[85] Z. Yan and Z. Wang, Tunable Weyl Points in Periodically Driven Nodal Line Semimetals, Phys. Rev. Lett. **117**, 087402 (2016).

[86] C.-K. Chan, Y.-T. Oh, J. H. Han, and P. A. Lee, Type-II Weyl cone transitions in driven semimetals, Phys. Rev. B **94**, 121106 (2016).

[87] A. Narayan, Tunable point nodes from line-node semimetals via application of light, Phys. Rev. B **94**, 041409 (2016).

[88] X.-X. Zhang, T. T. Ong, and N. Nagaosa, Theory of photoinduced Floquet Weyl semimetal phases, Phys. Rev. B **94**, 235137 (2016).

[89] K. Taguchi, D.-H. Xu, A. Yamakage, and K. T. Law, Photovoltaic anomalous Hall effect in line-node semimetals, Phys. Rev. B **94**, 155206 (2016).

[90] Y. Du, F. Tang, D. Wang, L. Sheng, E.-j. Kan, C.-G. Duan, S. Y. Savrasov, and X. Wan, CaTe: A new topological node-line and Dirac semimetal, npj Quant. Mater. **2**, 3 (2017).

[91] S. Kobayashi, Y. Yamakawa, A. Yamakage, T. Inohara, Y. Okamoto, and Y. Tanaka, Crossing-line-node semimetals: General theory and application to rare-earth trihydrides, Phys. Rev. B **95**, 245208 (2017).

[92] T. Bzdušek, Q. Wu, A. Rüegg, M. Sigrist, and A. A. Soluyanov, Nodal-chain metals, Nature (London) **538**, 75 (2016).

[93] R. Yu, Q. Wu, Z. Fang, and H. Weng, From nodal chain semimetal to Weyl semimetal in HfC, arXiv:1701.08502.

[94] Y. X. Zhao and Y. Lu, PT-Symmetric Real Dirac Fermions and Semimetals, Phys. Rev. Lett. **118**, 056401 (2017).

[95] F. Wilczek and A. Zee, Linking Numbers, Spin, and Statistics of Solitons, Phys. Rev. Lett. **51**, 2250 (1983).

[96] M. Nakahara, *Geometry, Topology and Physics* (CRC Press, Boca Raton, FL, 2003).

[97] E. Fradkin, *Field Theories of Condensed Matter Physics* (Cambridge University Press, Cambridge, UK, 2013).

[98] J. E. Moore, Y. Ran, and X.-G. Wen, Topological Surface States in Three-Dimensional Magnetic Insulators, Phys. Rev. Lett. **101**, 186805 (2008).

[99] D.-L. Deng, S.-T. Wang, C. Shen, and L.-M. Duan, Hopf insulators and their topologically protected surface states, Phys. Rev. B **88**, 201105 (2013).

[100] D.-L. Deng, S.-T. Wang, K. Sun, and L.-M. Duan, Probe knots and Hopf insulators with ultracold atoms, arXiv:1612.01518.

[101] D.-L. Deng, S.-T. Wang, and L.-M. Duan, Systematic construction of tight-binding Hamiltonians for topological insulators and superconductors, Phys. Rev. B **89**, 075126 (2014).

[102] R. Kennedy, Topological Hopf-Chern insulators and the Hopf superconductor, Phys. Rev. B **94**, 035137 (2016).

[103] C. Liu, F. Vafa, and C. Xu, Symmetry-protected topological Hopf insulator and its generalizations, Phys. Rev. B **95**, 161116 (2017).

[104] P. J. Ackerman and I. I. Smalyukh, Diversity of Knot Solitons in Liquid Crystals Manifested by Linking of Preimages in Torons and Hopfions, Phys. Rev. X **7**, 011006 (2017).

[105] C. Wang, P. Zhang, X. Chen, J. Yu, and H. Zhai, Measuring Topological Number of a Chern-Insulator From Quench Dynamics, Phys. Rev. Lett. **118**, 185701 (2017).

[106] Z. Yan, R. Bi, and Z. Wang, Majorana Zero Modes Protected by a Hopf Invariant in Topologically Trivial Superconductors, Phys. Rev. Lett. **118**, 147003 (2017).

[107] S. Ryu and Y. Hatsugai, Topological Origin of Zero-Energy Edge States in Particle-Hole Symmetric Systems, Phys. Rev. Lett. **89**, 077002 (2002).

[108] Note that Π_x, Π_y do not commute. We take the symmetric ordering for operators, e.g., $k_x k_y^2 \rightarrow (\Pi_x \Pi_y \Pi_y + \Pi_y \Pi_x \Pi_y + \Pi_y \Pi_y \Pi_x)/3$.

[109] G. P. Mikitik and Yu. V. Sharlai, Manifestation of Berry's Phase in Metal Physics, Phys. Rev. Lett. **82**, 2147 (1999).

[110] L. Onsager, Interpretation of the de Haas-van Alphen effect, Phil. Mag. **43**, 1006 (1952).

[111] D. Xiao, M.-C. Chang, and Q. Niu, Berry phase effects on electronic properties, Rev. Mod. Phys. **82**, 1959 (2010).

[112] See Supplemental Material at http://link.aps.org/supplemental/10.1103/PhysRevB.96.041103 for technical details of calculations.

[113] N. H. Lindner, G. Refael, and V. Galitski, Floquet topological insulator in semiconductor quantum wells, Nat. Phys. **7**, 490 (2011).

[114] T. Kitagawa, T. Oka, A. Brataas, L. Fu, and E. Demler, Transport properties of nonequilibrium systems under the application of light: Photoinduced quantum Hall insulators without Landau levels, Phys. Rev. B **84**, 235108 (2011).

[115] T. Oka and H. Aoki, Photovoltaic Hall effect in graphene, Phys. Rev. B **79**, 081406 (2009).

[116] J.-i. Inoue and A. Tanaka, Photoinduced Transition between Conventional and Topological Insulators in Two-Dimensional Electronic Systems, Phys. Rev. Lett. **105**, 017401 (2010).

[117] Z. Gu, H. A. Fertig, D. P. Arovas, and A. Auerbach, Floquet Spectrum and Transport through an Irradiated Graphene Ribbon, Phys. Rev. Lett. **107**, 216601 (2011).

[118] T. Kitagawa, M. S. Rudner, E. Berg, and E. Demler, Exploring topological phases with quantum walks, Phys. Rev. A **82**, 033429 (2010).

[119] T. Kitagawa, E. Berg, M. Rudner, and E. Demler, Topological characterization of periodically driven quantum systems, Phys. Rev. B **82**, 235114 (2010).

[120] L. Jiang, T. Kitagawa, J. Alicea, A. R. Akhmerov, D. Pekker, G. Refael, J. I. Cirac, E. Demler, M. D. Lukin, and P. Zoller, Majorana Fermions in Equilibrium and in Driven Cold-Atom Quantum Wires, Phys. Rev. Lett. **106**, 220402 (2011).

[121] M. S. Rudner, N. H. Lindner, E. Berg, and M. Levin, Anomalous Edge States and the Bulk-Edge Correspondence for Periodically Driven Two-Dimensional Systems, Phys. Rev. X **3**, 031005 (2013).

[122] B. Lian, C. Vafa, F. Vafa, and S.-C. Zhang, Chern-Simons theory and Wilson loops in the Brillouin zone, Phys. Rev. B **95**, 094512 (2017).

[123] W. Chen, H.-Z. Lu, and J.-M. Hou, Topological semimetals with a double-helix nodal link, Phys. Rev. B **96**, 041102 (2017).

[124] M. Ezawa, Topological semimetals carrying arbitrary Hopf numbers: Fermi surface topologies of a Hopf link, Solomon's knot, trefoil knot, and other linked nodal varieties, Phys. Rev. B **96**, 041202 (2017).